

composition offer insights into the trends in mechanical properties.

Since most Laves phases are brittle at room temperature, mechanical testing is severely limited. Microcracks that form during processing and sample preparation are not uncommon. Thus, the testing of large samples may not be truly representative, and may underestimate the true potential of Laves phases. Microindentation probes only a small polished area, and thereby eliminates many of the problems associated with bulk testing. Hardness values are measures of the resistance to plastic deformation, and are established as a function of alloy composition in this study. In addition, fracture toughness represents the resistance to cracking, and is determined from crack lengths around indent impressions. Microindentation has previously discerned compositional effects on the hardness and fracture toughness of TiCr_2 Laves phase alloys [9].

Relative to the “perfect” stoichiometric lattice, defects (e.g. excess atoms, alloying additions, or vacancies) alter the unit cell dimensions, atomic bonding, and phase stability of the Laves phases. Furthermore, these changes can also affect the way in which the atoms move during deformation. The passage of dislocations in the Laves structure requires a “synchroshear” mechanism [10]. Successive layers of close-packed atoms must *synchronously* swap atomic positions in order for dislocations to move through the crystal, while maintaining crystal symmetry. Thus, the deformability of Laves phase intermetallics is intrinsically related to the atomic structure and environment.

2. Experimental procedures

The HfCo_2 alloy samples were arc-cast with nominal compositions from Hf-64 (at.%) Co to Hf-73 (at.%) Co. Heat treatments were performed at 1200 °C for 100 h, followed by 1400 °C for 100 h, and slow cooled. Compositions were determined by electron probe microanalysis (EPMA), and crystal structures were confirmed by X-ray diffraction (XRD). Density measurements were performed on single-phase samples by water immersion. Characterizations of the as-cast and heat-treated polycrystalline alloys are documented in Part I of this paper [2]. Specimens were prepared for transmission electron microscopy (TEM) by cutting 3 mm discs with a coring saw, followed by dimpling and ion milling. Dislocation analyses were performed with a Philips CM30 operating at 300 kV.

Heat-treated, single-phase C15 samples on both sides of the HfCo_2 stoichiometry were selected for elastic constant measurements by RUS. Specimens were cut and polished into small parallelepipeds. Details of the RUS set-up and technique can be found elsewhere [3,6]. Forty peaks in the range of 0.2–0.8 MHz at room tem-

perature were used in this study. The r.m.s. errors for the fitting of all 40 peaks were less than 0.6% for all the samples, and indicate a good agreement between the experimental and calculated resonances.

The elastic constants were determined numerically by solving the inverse problem since the resonant frequencies are dependent upon the sample’s elastic constants, dimensions, and density. The dimensions and density of each sample are determined experimentally, and then the elastic constants are estimated. Resonant frequencies are calculated, and a figure of merit is defined to compare the measured and calculated frequencies. A systematic and iterative method is employed to generate the elastic constants to high accuracy.

The hardness and fracture toughness measurements were performed at room temperature on a Micromet microhardness tester with a Vickers indenter. A load of 500 g and dwell time of 15 s were used. Ten or more indentations were made on each alloy sample. Measurements of impression diagonals and crack lengths were made under consistent high magnifications with scanning electron microscopy (SEM). Hardness values (H) [11] and fracture toughness values (K) [12] were computed from the following equations:

$$H = 1854.4 P/d^2 \quad (1)$$

$$K = 0.016 (E/H)^{1/2} (P/c^{3/2}) \quad (2)$$

where P is the load (g), d is the mean impression diagonal (μm), and c is the average crack length (μm). A Young’s modulus value (E) of 209.4 GPa from the RUS measurements was used in the analyses.

3. Results

3.1. Elastic constants

Fig. 1 shows a portion of the room temperature RUS spectrum of the Hf-67.4 Co sample. Table 1 compares resonance peak positions (f_{expt}) found in Fig. 1 and the corresponding calculated values (f_{calc}), and shows good matching. The Young’s modulus (E), bulk modulus (B), shear modulus (G), Poisson’s ration (ν), and Debye temperature (Θ_D) for two Hf-rich and two Co-rich HfCo_2 alloy compositions are listed in Table 2.

An interesting trend with the Young’s modulus and bulk modulus as a function of composition is revealed in Fig. 2. A maximum in both moduli appears to occur near the stoichiometric Laves phase composition (Hf-66.7 Co). Straight lines are drawn through the Hf-rich HfCo_2 data points and through the Co-rich HfCo_2 data points in order to calculate the maximum. Extrapolated values of the composition and modulus corresponding to these maximums are listed in Table 3.

The shear modulus (G) is plotted as a function of composition in Fig. 3. A distinct maximum does not appear, as with the elastic and bulk modulus. The data points vary only about 1.5%. However, a break does occur between the Hf-rich and Co-rich sides of the HfCo_2 stoichiometry, with each side fairly constant. The shear modulus drops in value as the Laves phase composition becomes Co-rich.

Table 1
Data fitting for a portion of the room temperature RUS spectrum (Fig. 1) of the Hf-67.4Co alloy; the experimental resonance, f_{expt} , is compared with the calculated resonance, f_{calc}

No.	f_{expt} (kHz)	f_{calc} (kHz)	Error (%)
1	711.000	706.549	-0.63
2	725.070	720.011	-0.70
3	761.150	767.108	0.78
4	793.230	792.644	-0.07
5	801.960	802.901	0.12
6	833.910	829.749	-0.50
7	885.660	893.217	-0.85
8	896.790	896.923	0.01

Table 2
Elastic constants determined by resonant ultrasound spectroscopy (RUS) of HfCo_2 Laves phases

Laves composition (at.% Co)	E , Young's modulus (GPa)	B , bulk modulus (GPa)	G , shear modulus (GPa)	ν , Poisson's ratio	Θ_D , Debye temperature (K)
65.5	204.57	168.95	78.79	0.2982	362.65
66.1	207.92	191.25	78.83	0.3185	366.29
67.4	209.41	220.41	77.96	0.3418	369.46
70.6	203.78	181.28	77.62	0.3126	371.22

Fig. 4 shows the compositional dependence of the Poisson's ratio (ν). Again, a maximum is found near the stoichiometric composition (Table 3). The Debye temperature (Θ_D) is plotted as a function of Laves phase composition in Fig. 5. As the Co-content increases, the Debye temperature also increases.

3.2. Mechanical properties

Fig. 6 is a SEM image of a typical Vickers indent. Cracks radiate out from the corners of the indentation impression. The sets of as-cast and heat-treated samples are tested and measured under similar conditions. The microhardness values are plotted against alloy composition in Fig. 7. For almost each alloy composition, the hardness values from the two conditions are within error bars. However, the hardness values of the heat-treated samples are generally higher than the as-cast alloys. The as-cast alloys are not as compositionally homogeneous as the heat-treated samples. Nevertheless, the overall trend of the hardness with respect to alloy composition is identical for the as-cast and heat-treated alloys.

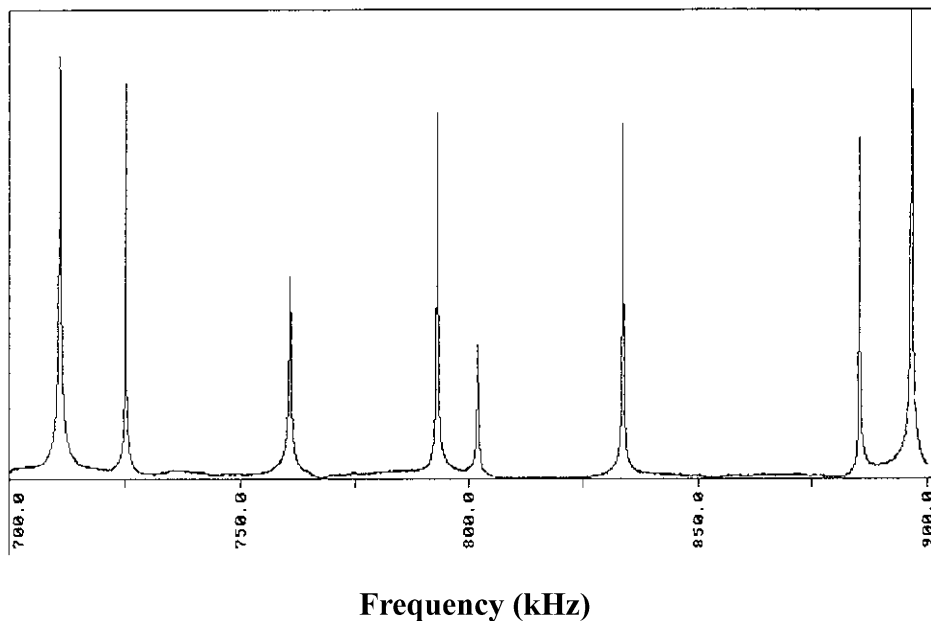


Fig. 1. A portion of the room-temperature resonant frequency (RUS) spectrum of C15 HfCo_2 .

Two different phase fields are represented on the plot in Fig. 7. The most Hf-rich alloys (open data points) actually occur within the two-phase field of $\text{HfCo} + \text{HfCo}_2$ [2]. Although the indents are deliberately directed in the HfCo_2 areas of the two-phase alloys, only the surface can be seen. Presumably, HfCo particles beneath the surface are being included in the measurements, and account for the decrease in hardness values as the alloys become more Hf-rich.

Within the single-phase HfCo_2 field (i.e. filled data points), the hardness is dependent upon the composition. A maximum occurs around the stoichiometric Laves composition (i.e. Hf-66.7 at.% Co). A steady

decrease in hardness accompanies the deviation from stoichiometry, and is readily apparent on the Co-rich side of stoichiometry.

Crack measurements for fracture toughness assessment are made only on the single-phase HfCo_2 samples. The two-phase microstructures of the Hf-rich alloys are too coarse for the indentation to be truly representative of the two-phase structure. Furthermore, the second phase particles of HfCo often interfere with crack propagation (Fig. 8), and lead to inconsistent crack patterns.

Fig. 9 displays the fracture toughness values for the as-cast and heat-treated samples as a function of Laves phase composition. The heat-treated values are consistently higher than those of the as-cast alloys. The annealing treatment most likely alleviates the residual stresses created from the initial processing and also homogenizes the alloys. For both conditions, slight improvements in the toughness correlate with the Co-rich compositions. The fracture toughness values are quite low, and confirm that monolithic HfCo_2 Laves phases are indeed brittle at room temperature.

While the differences in fracture toughness are not considerable, use of an index of brittleness, (the ratio of hardness to fracture toughness, H/K) [13], can distinguish

Table 3
Extrapolated Laves phase composition and elastic constant values from the intersection of compositional (Hf-rich and Co-rich) dependent experimental values. The maximum of the constants occur near the stoichiometric composition

Elastic constant	Laves phase alloy composition (at.% Co)	Calculated value (GPa)
E , elastic modulus	66.61	210.79
B , bulk modulus	67.01	225.17
ν , Poisson's ratio	66.92	0.3462

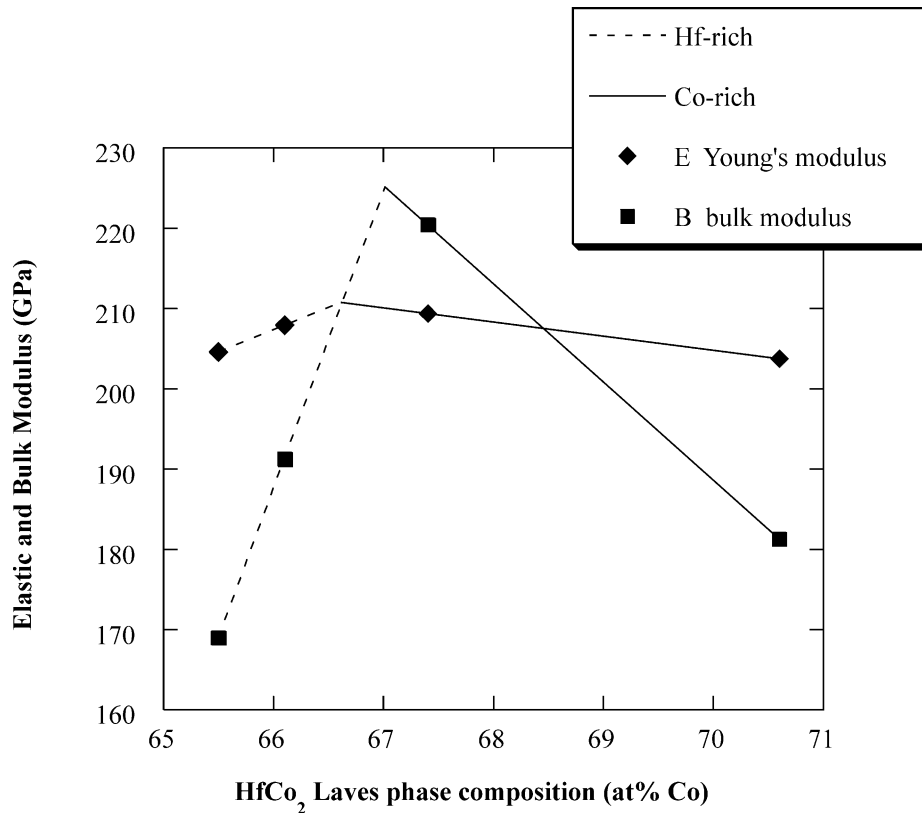


Fig. 2. The Young's (E) and bulk (B) moduli as a function of HfCo_2 Laves phase composition. The Hf-rich and Co-rich relationships intersect at a maximum near the stoichiometric Laves composition.

clear trends in Fig. 10. A decrease in the brittleness occurs as Laves compositions deviate from stoichiometry and become more Co-rich. The Hf-rich composition actually demonstrates greater brittleness than the stoichiometric alloy. The brittleness of the as-cast alloys are not plotted in the figure, and are much greater than the heat-treated alloys ($\sim 10\text{--}11 \mu\text{m}^{-1/2}$), while showing the same trends.

4. Discussion

4.1. Elastic properties

Caution is warranted in relating the elastic properties to the mechanical behavior. The indentation impressions and cracks result from plastic deformation of the material. However, the flow stresses required for deformation

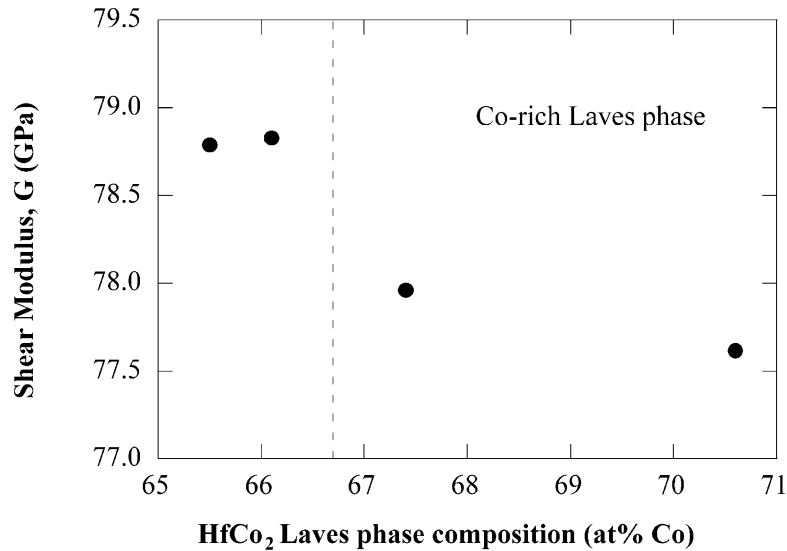


Fig. 3. The shear modulus (G) as a function of HfCo₂ Laves phase composition.

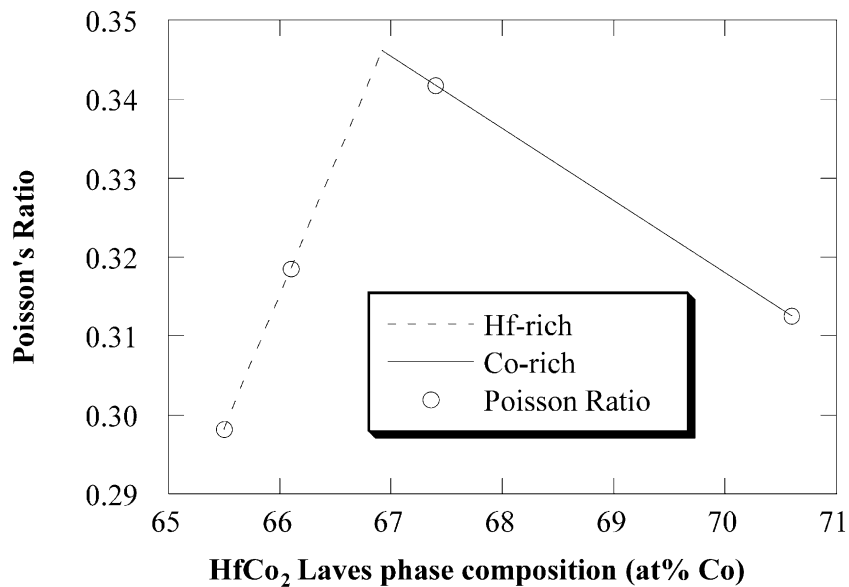


Fig. 4. Poisson's ratio (ν) as a function of the HfCo₂ Laves phase composition.

are related to the elastic properties since atomic bonds are stretched and distorted. Plastic-elastic models are often used to describe the stress states due to indentation, since the deformed regions are constrained by elastic material. Moreover, the driving force for material fracture is related to the accompanying elastic energy release [14]. In this study, the elastic constants determined by RUS are used to help understand the bonding and structure of the material, which in turn, play a key role in the trends in the mechanical properties.

Table 4 lists the elastic constants of other $C15$ Laves phases determined by RUS. The elastic constants of $HfCo_2$ are very similar to those of $NbCr_2$, yet different from the HfV_2 -base alloys. The higher modulus values of $NbCr_2$, with respect to $HfCo_2$, are in accordance with a higher melting temperature (and thus stronger bonding) of $NbCr_2$. The HfV_2 alloys also show anomalous behavior where the Young's modulus (E) and shear (G) modulus increase with increasing temperature [6]. The exact origin of the low elastic moduli of HfV_2 and

Table 4
Elastic constants determined by RUS for different $C15$ Laves phases

Laves phase	E (GPa)	B (GPa)	G (GPa)	ν
$HfCo_2^a$	209.4	220.4	78.0	0.34
$NbCr_2$	214.1	229.4	79.6	0.34
HfV_2	104	82	30	0.38
$HfV_2 + Nb^b$	146.1	84.4	30.1	0.40

^a $HfCo_{67.4}$.

^b $Hf_{25}V_{60}Nb_{15}$.

Table 5
Elastic moduli and Poisson's ratio for $HfCo_2$, its constituent elements, and values from the rule of mixtures

Material	E (GPa)	G (GPa)	B (GPa)	ν
Hf [15]	143	56	109	0.28
Co [16]	211	82	182	0.32
$HfCo_2$ (rule of mixtures)	188	73	158	0.31
$HfCo_2$ (RUS results)	209	78	229	0.34

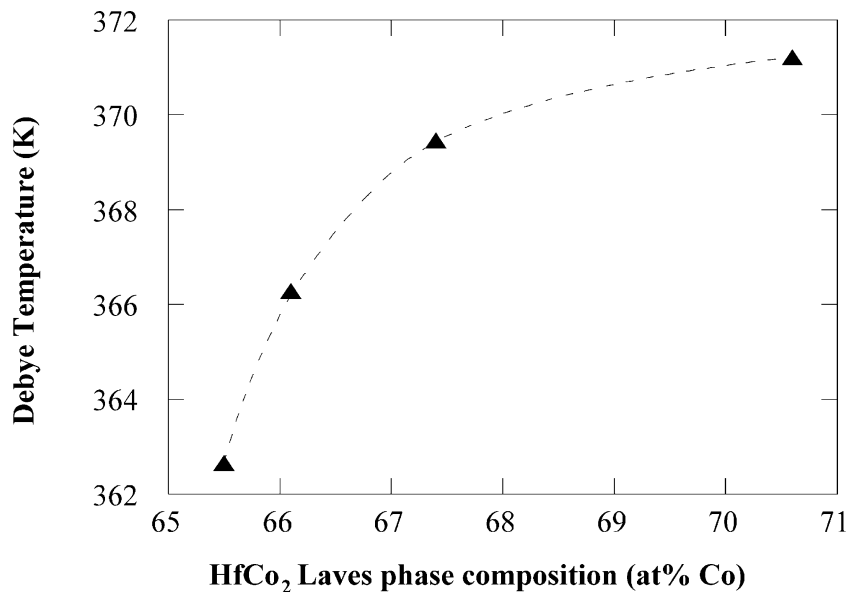


Fig. 5. The Debye temperature (Θ_D) increases as the Co-content of the $HfCo_2$ Laves phase increases.

HfV₂+Nb are still under investigation. Building upon the growing compilation of Laves phase RUS elastic constants [6,7], HfCo₂ can be considered “normal”, rather than “anomalous”. The enhanced room temperature deformation found with the HfV₂-base

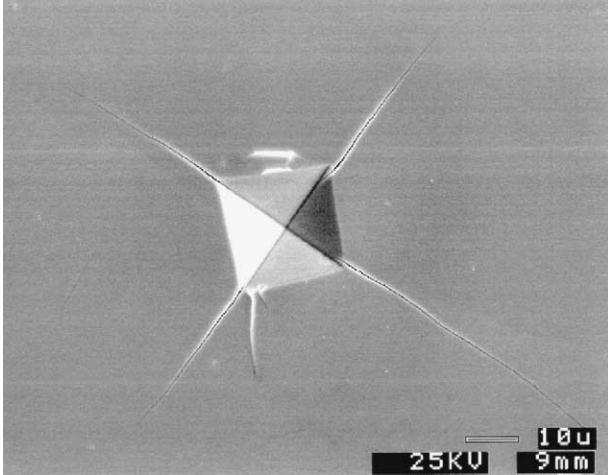


Fig. 6. SEM micrograph of an indentation on the C15 Hf-69.9Co Laves phase alloy.

Laves phase alloys may be related to its anomalous elastic properties. Correspondingly, the mechanical properties of HfCo₂ and NbCr₂ appear to be similar in respect to the limited deformability compared to HfV₂ [15,16].

The elastic properties of C15 HfCo₂ alloys have some notable features. The shear modulus (~78 GPa) is low, close to those of transition metals. The value is much lower than those of other high-temperature structural intermetallics. The Poisson’s ratio is also close to those of transition metals (~1/3), but higher than those of high-temperature structural intermetallics. The combination of these two features indicate that the HfCo₂ Laves phase alloys do not have much interatomic bonding directionality and may have some degree of deformability.

Table 5 lists the experimentally determined elastic moduli and Poisson’s ratios for HfCo₂ and its constituent elements, Hf and Co [17,18]. The values from a rule of mixtures is also computed (Table 5) and compared to the RUS results. The shear modulus of HfCo₂ is close to the value from the rule of mixtures. However, the other elastic constants are significantly higher than the predicted mixture values. The same observations hold for NbCr₂ [7], but not for the HfV₂ alloys [6].

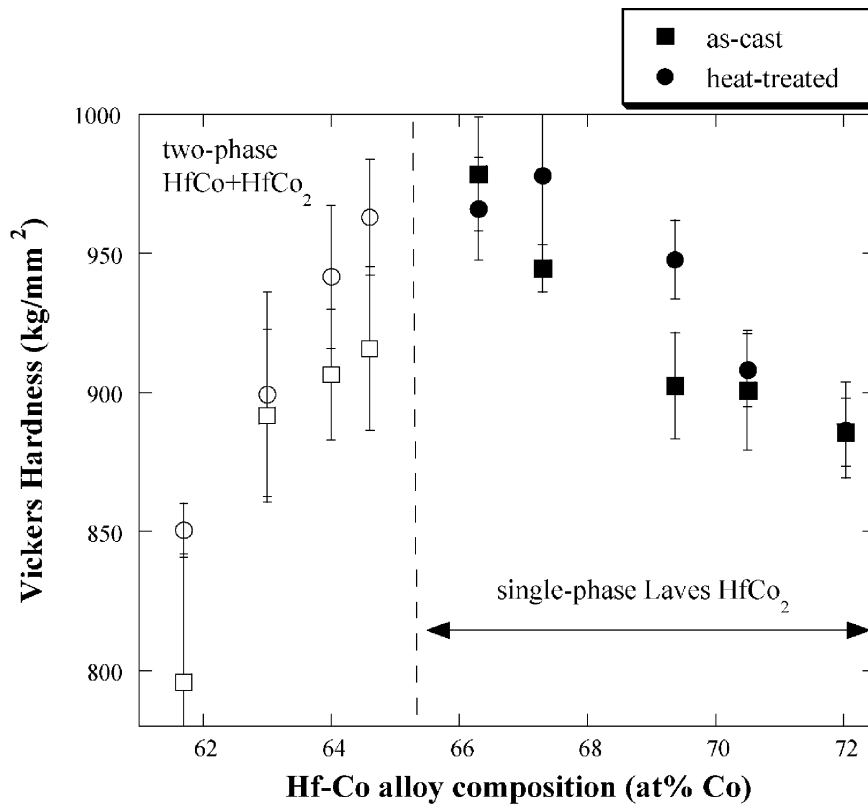


Fig. 7. The room-temperature hardness of Hf-Co alloys (at a load of 500 g). The maximum hardness occurs around the stoichiometric HfCo₂ composition.

The Debye temperature is related to the characteristic maximum vibration frequency of the atoms. As the Co-content of the HfCo_2 alloy increases, the Debye temperature increases, indicating greater vibration frequencies that can be correlated with smaller atomic packing efficiency within the structure. The ramifications are discussed later with respect to deformation.

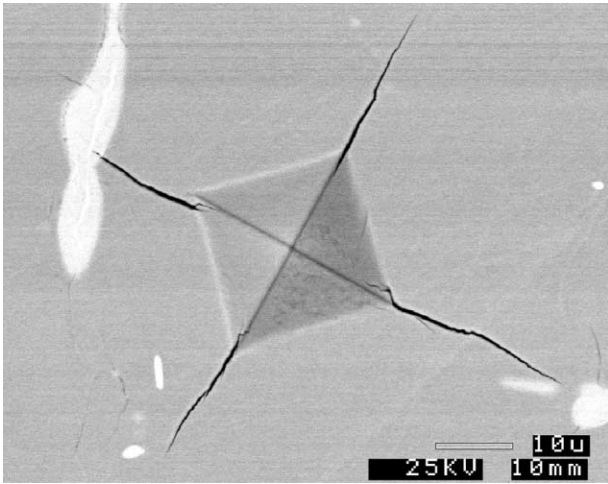


Fig. 8. Back scattered electron image of the crack interaction with a second phase particle (HfCo) in a Hf-rich, two-phase Hf-Co alloy sample.

4.2. Compositional trends

The maximums found in the Young's modulus (E) and bulk modulus (B) near the stoichiometric HfCo_2 compositions are reasonable in the sense that the Laves phase has the most "perfect" lattice structure at stoichiometry. Consequently, bonding should be the strongest and most rigid. Indeed, the microhardness results concur with the largest values near stoichiometry. Increasing off-stoichiometric compositions, in both the Hf-rich and Co-rich directions, scale with decreasing E and B .

The decrease in hardness with deviation from Laves phase stoichiometry is also reported in the TiCr_2 [9], MgZn_2 [19], and NbFe_2 [20] Laves phase systems. These observations are opposite to the trend in most other intermetallics. Generally, nonstoichiometric intermetallic compositions lead to increased hardness at low homologous temperatures [21]. Solid solution hardening in dilute alloys and intermetallics is explained in terms of elastic interactions of the solute atom or defect with dislocations [22]. Constitutional defects in intermetallics are thought to interfere with dislocation movement, and thus produce hardening. At higher homologous temperatures, these defects assist diffusion and dislocation climb, causing a softening effect. However, nonstoichiometric defects in the Laves phases correlate with improved deformability at room temperature. (Studies involving high-temperature hardness tests on HfCo_2

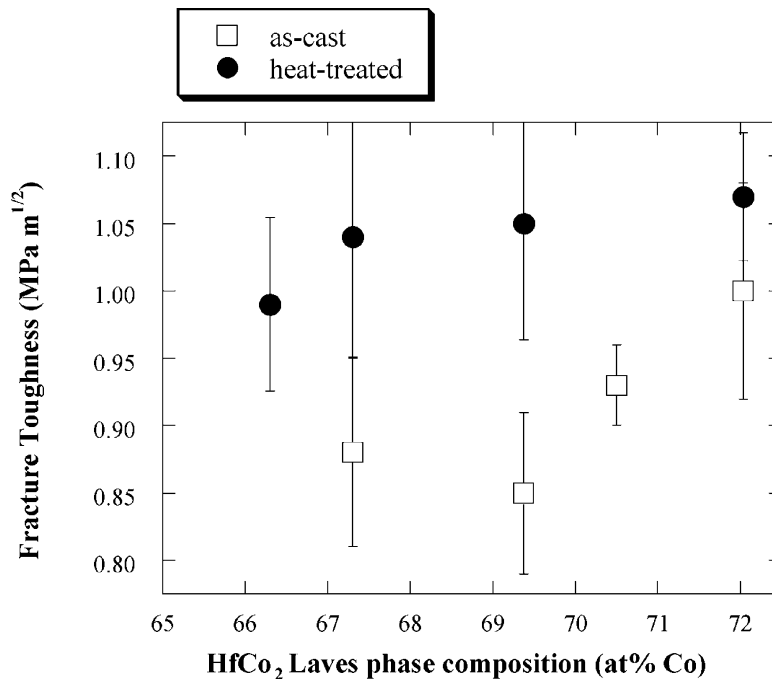


Fig. 9. Fracture toughness as a function of the HfCo_2 Laves phase composition.

alloys are forthcoming.) The presence of more defects and dislocations in the nonstoichiometric Laves phases is proposed to explain the softening effect in hardness values [19]. Deviation from the “perfect lattice”, may actually aid the deformation of Laves phases. The interaction of defects with dislocations may be unique to the class of Laves phase intermetallics. Since the compositional dependencies in the hardness of the Laves phases differ with those of other intermetallics, the Laves phases may also possess different strengthening or ductilizing mechanisms.

Improvements in the deformability and toughness are associated with the off-stoichiometric HfCo_2 alloys. The brittleness decreases as the alloy compositions become more Co-rich (Fig. 10). Increases in fracture toughness are also associated with deviation from the TiCr_2 stoichiometry [9]. Thus, constitutional defects in the Laves phases may aid the deformation process. Vacancies are also suggested to assist the movement of partial dislocations in Laves phases [23], although are not considered to play a large role in HfCo_2 [2].

Sizes of the atoms are often used to understand the deformation process. Alloying additions that decrease the effective radius ratio, r_A/r_B , of AB_2 Laves phases (e.g. smaller atoms on the A-sublattice) have been proposed to facilitate shear deformation [24,25]. Similar toughening strategies exist whereby an alloying addition of element, C, should have a size in between that of the A and B host atoms (i.e. $r_A > r_C > r_B$), in order to occupy both

sublattices [13]. $\text{HfV}_2 + \text{Nb}$ [15], $\text{NbCr}_2 + \text{Mo}$ [25], and $\text{TiCr}_2 + \text{Mo}$ [9] are all such examples where deformation appears to improve upon alloying. Consistent with the above ideas, excess Co atoms on the Hf-sublattice [2], result in improved deformability.

The shear modulus is also associated with the improved deformation of the Co-rich HfCo_2 alloys. The Rice–Thomson criterion is an indicator of ductile alloy behavior when Gb/γ is small (where b is the magnitude of the Burgers vector and γ is the surface energy) [26]. Thus, lowering the shear modulus (G) could improve the deformability. A slight decrease in G is correlated with the Co-rich compositions (Fig. 3), and may allow easier deformation that is manifested in the lower hardness and greater toughness values.

4.3. Deformation and synchroshear

Laves phases are topologically close-packed (TCP) structures in which the A and B atoms are arranged for the maximum packing efficiency. Fig. 11 [27] displays the basic layer unit of the Laves phase, and comprises of four atomic close-packed planes. Variations in the stacking sequences of these layer units create the different Laves crystal structures ($C14$, $C36$, and $C15$). Layer A in Fig. 11 is a *Kagome* net of the smaller B atoms, and a pair of A atoms (in a dumbbell-like configuration), within the α layers, fits inside the openings of the *Kagome* net. Fig. 12 illustrates the layering of close-

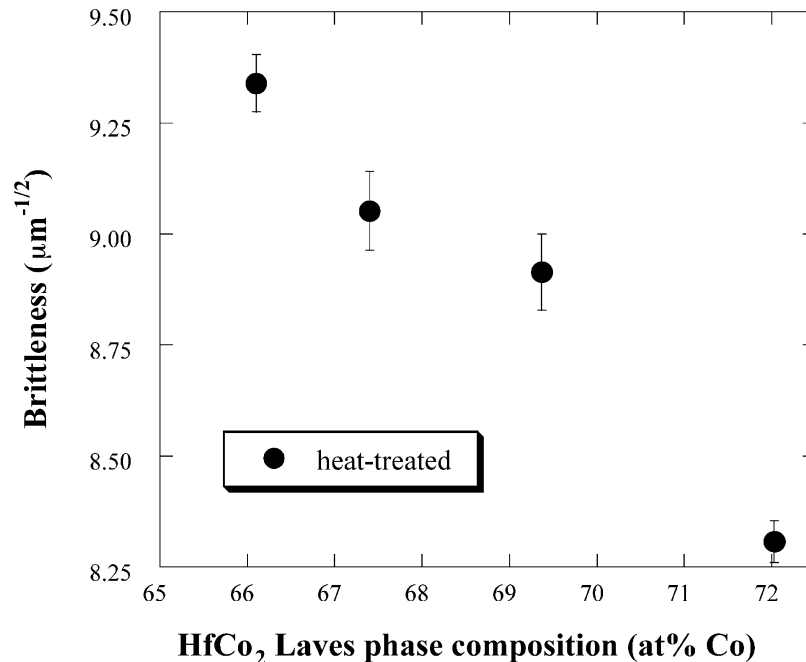


Fig. 10. Brittleness (H/K) of the heat-treated HfCo_2 Laves phases decreases with Co-content.

packed planes that build up the C15 Laves structure. The atom radii are reduced in the figure for unobstructed viewing, since in the hard sphere model with the ideal radius ratio, the A atoms contact each other but not any of the B atoms, and vice versa.

The slip system of the C15 Laves phase is $\{111\}(110)$. Dislocation movement occurs within the close-packed layers that contain the least amount of atoms and that do not contain the “dumbbell” of A atoms. Thus for example, the “ $\alpha\zeta\beta$ ” layers of the C15 structure in Fig. 12

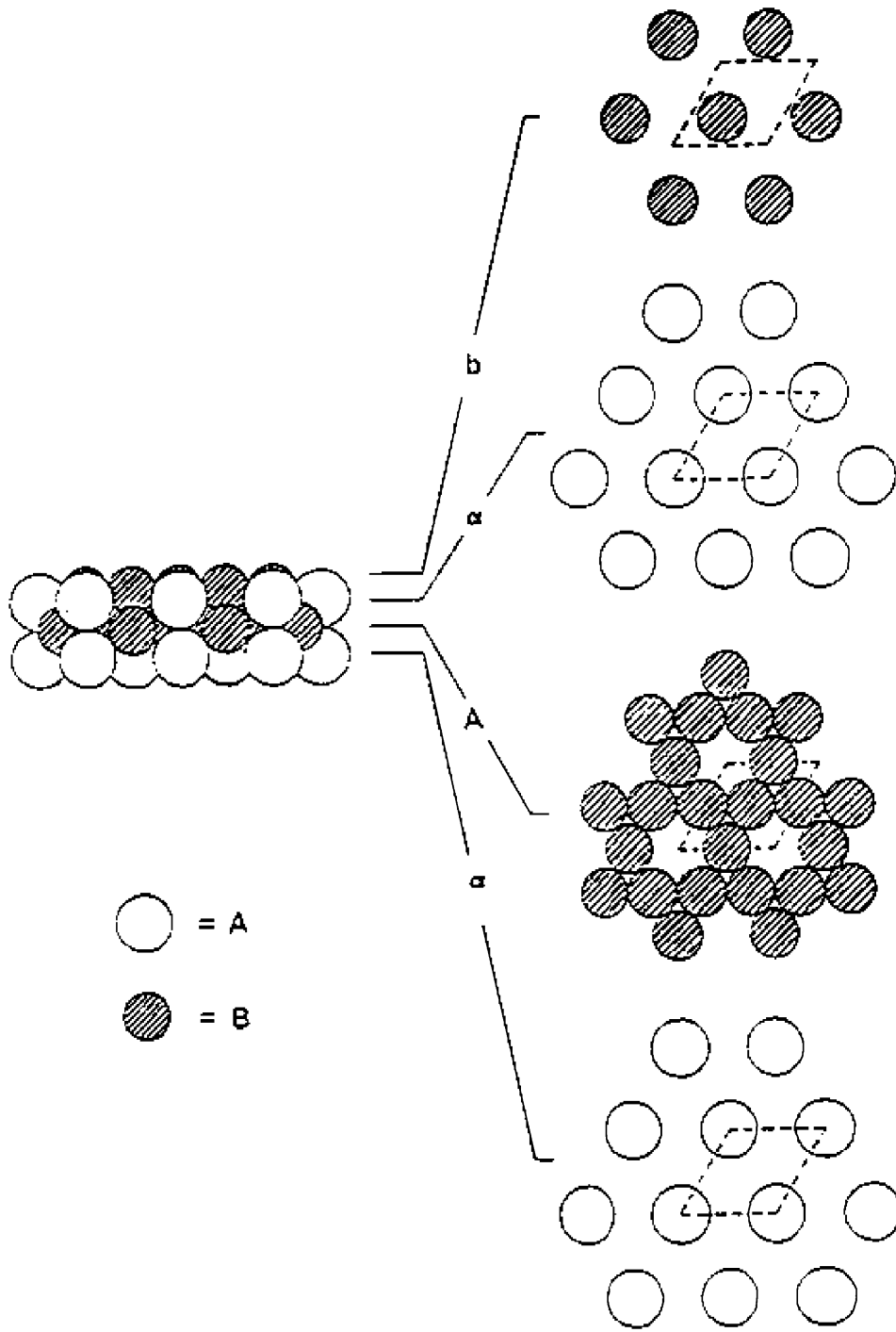


Fig. 11. The basic four-layer stacking unit (consisting of the close-packed planes) used to build up the different Laves phase crystal structures. The Greek symbols denote the position of the A atoms. Placement of the B atoms are marked by the Roman letters, where the capital letters represent the dense Kagome net, and the small Roman letters represent the less dense layer. [26].

are the active atomic layers in the synchroshear mechanism. Due to the TCP nature of the Laves phases, synchronous movement of adjacent atomic layers is required for the passage of dislocations or partial dislocations. One layer of atoms (e.g. c) may shear by $1/6 [\bar{2}11]$ if at the same time, the next and adjacent layer (i.e. β) shears by $1/6 [\bar{1}\bar{2}\bar{1}]$. The following sequence results:

$$1/6[\bar{2}11] + 1/6[\bar{1}\bar{2}\bar{1}] = 1/2[\bar{1}10] \quad (3)$$

and crystal symmetry is also preserved. Fig. 13 displays the weak beam TEM analysis of a dissociated dislocation and its partials. The schematic indexes the dislocation and partials, and is consistent with the synchroshear mechanism.

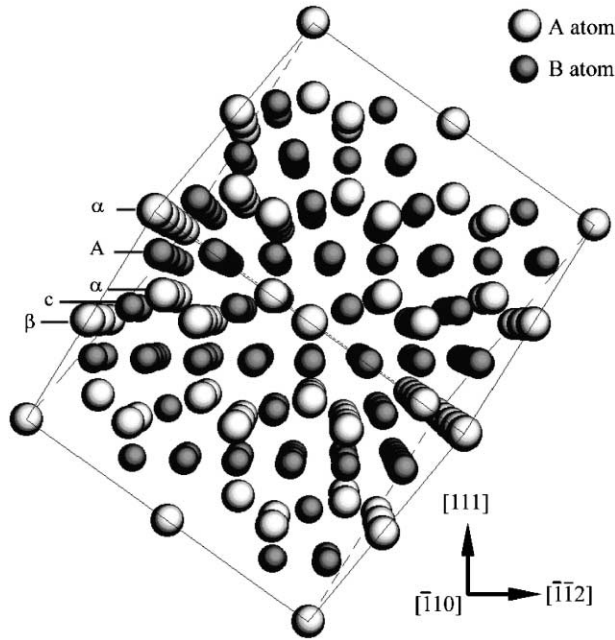


Fig. 12. Schematic of the stacking of (111) planes in the C15 Laves phase structure. The $\alpha\beta$ layers, rather than the $\alpha\alpha$ layers, are involved in synchroshear.

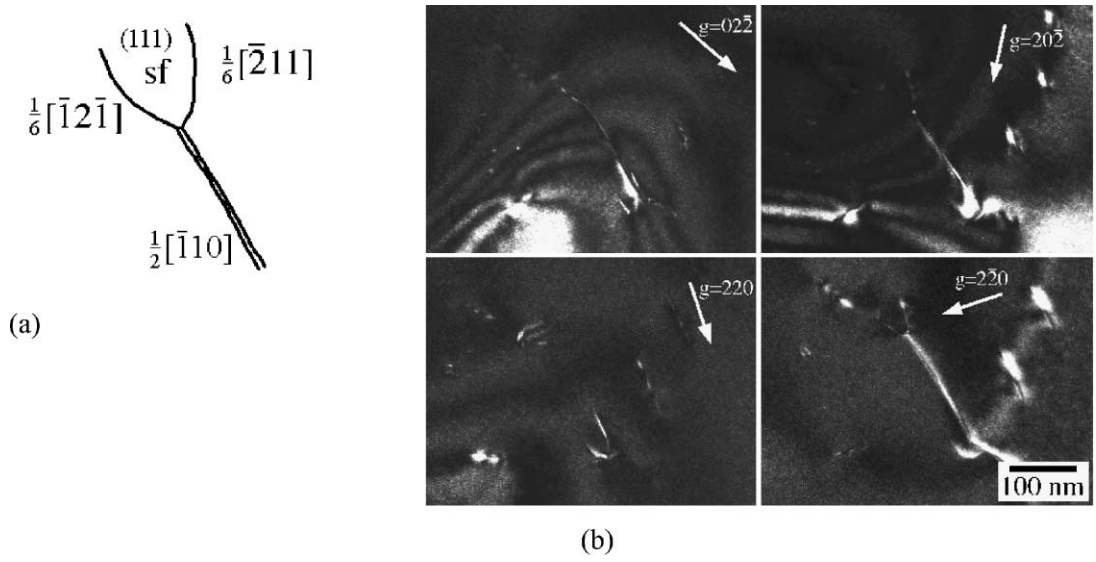


Fig. 13. (a) Indexed schematic and (b) TEM images of dislocation analysis (partials, stacking fault, and undissociated dislocation) in HfCo_2 .

The ease in which synchroshear can proceed affects deformation behavior and the mechanical properties. The “free” volume within the synchroshear layers (i.e. $\alpha\beta$) is thought to control the ability in which atoms can move in shear deformation [24]. In order to comprehend the effects on synchroshear, the atoms are treated as rigid spheres. Vacancies or atomic substitutions, which decrease the atom packing efficiency of the synchroshear layers, can then facilitate the atomic movements in the synchroshear process. However, introduction of vacancies or anti-site substitutions will also affect the unit cell size (i.e. the lattice constant). Thus, the effects of changing the lattice size must be weighed against the effects of changing the atomic constituents (or total atomic volume) within the structure. For example, in the case of B-rich Laves phase compositions, excess (and smaller) B atom on the A-sublattice may decrease the total atomic volumes, but will also decrease the entire lattice size. Consequently, the atomic packing factor (APF) is determined and is simply the total volume of atoms in unit cell divided by the volume of the unit cell (as calculated from experimental XRD lattice constants).

The atomic packing factors were determined for the different HfCo_2 alloy compositions in this study. Anti-site substitutions are assumed for the nonstoichiometric compositions and experimental lattice constants are used [2]. The APFs were normalized with respect to the stoichiometric value, and are plotted in Fig. 14. Evidently, the changes in atomic volumes are greater than the changes in lattice constants as a function of HfCo_2 composition. The relative APF decreases as Co-atoms

are substituted onto the Hf-sublattice, and such a trend is consistent with the increase in atomic vibration frequencies or the Debye temperature (Fig. 5). More “open” space is created within the lattice as the compositions become Co-rich. Decreases in hardness and increases in fracture toughness are also correlated with the Co-rich HfCo_2 alloys. Thus, deviation from stoichiometry, by anti-site substitution of the smaller Co atom onto the Hf-sublattice, results in the decrease of the atomic packing, or in greater “open” or “free” volume. The atomic motions involved in synchroshear become easier, and the enhanced dislocation activity results in the improved deformation manifested by the mechanical properties.

While such a construct is useful, atoms are not hard spheres, and other factors, such as electronic structure and bonding, should also be considered. Since the strength of Laves phases originate from the tight packing and bonding of the dissimilar-sized atoms, any disorder to that structure would logically tend to decrease the hardness and possibly improve the deformation. On a local level, an anti-site substitution represents a “wrong” atom on a particular sublattice and disrupts the close-packing of atoms in a “perfect” TCP lattice. Around the misplaced atom, the immediate environment resembles the elemental metal. Conceivably, more metallic bonding is created locally, and more deformability ensues.

For example, the B atom has 12 surrounding A atoms as its nearest neighbors. An anti-site substitution of an A atom on the B sublattice would result in the metallic

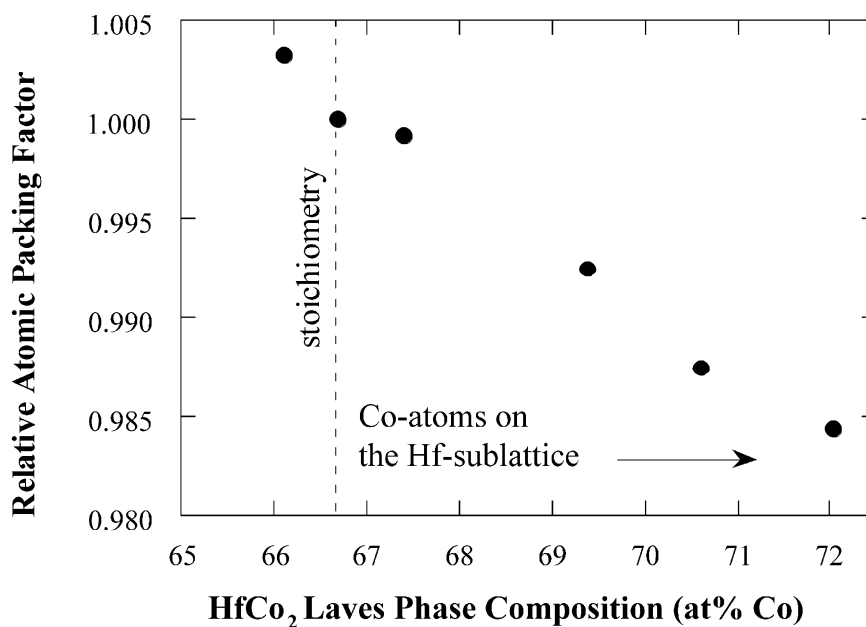


Fig. 14. The relative atomic packing factor (atomic volumes/lattice volume) as a function of HfCo_2 Laves phase composition.

coordination number of 12 for that particular A atom. On the other hand, an anti-site B atom on the A sublattice would result in having all B atoms in the vicinity of the synchroshear layer. Less charge transfer would occur around these “defect areas”, and more metallic bonding is possible. Elemental Co is relatively deformable, and the Co-rich HfCo₂ Laves phases appear to be less brittle.

4.4. Toughening strategies

The established structure–property relationships allow for the development of specific alloying methodologies to improve the toughness of Laves phases with sound and fundamental rationale. The notion that some disorder to the crystal lattice may assist deformation leads to attempts to widen the Laves phase field, through material system selection, processing routes [28], and/or alloying [29,30]. While nonstoichiometric Laves compositions demonstrate improved deformability, appropriate alloying additions can have even greater effects. Due to the size influences on Laves phase stability [31], an intermediate-sized alloying addition (i.e. $r_A > r_C > r_B$) can greatly extend the phase field out into ternary space. The effects of alloying additions on the APF, bonding character, and electronic structure of the Laves phase should also be considered. Such strategies have been employed with some success [29], and results from this study should help with future developments.

5. Conclusions

Several different aspects of the C15 HfCo₂ Laves phase structure were examined with regards to the effects on deformation. The room temperature elastic constants, E , B , G , ν and Θ_D , were determined as a function of composition by resonant ultrasound spectroscopy (RUS). Hardness and fracture toughness, by Vickers indentation at room temperature, were also assessed as a function of composition. From the understanding of structure-property relationships, alloying methodologies to improve deformability are then proposed.

1. The Young’s modulus, bulk modulus, and Poisson’s ratio appear to have a maximum near the stoichiometric HfCo₂ Laves composition.
2. The shear modulus is slightly lower for the Co-rich Laves compositions, and the Debye temperature continuously increases with Co-content of HfCo₂.
3. Contrary to most other classes of intermetallics, the HfCo₂ Laves phase alloys display a maximum in hardness near the stoichiometric composition at room temperature. Nonstoichiometric composi-

tions (or constitutional defects) correlate with decreases in hardness.

4. Fracture toughness and brittleness (H/K) improve with the off-stoichiometric, Co-rich HfCo₂ Laves compositions. Excess Co atoms on the Hf-sublattice results in lower atomic packing factors, and enhanced synchroshear deformation.
5. Based upon this study, toughening strategies could involve disrupting the “perfect” lattice and decreasing the atomic packing factor through expanding the Laves phase field and achieving nonstoichiometric Laves compositions by proper processing and alloying conditions.

References

- [1] Livingston JD. *Phys Stat Sol (a)* 1992;131:415.
- [2] Chen KC, Peterson EJ, Thoma DJ. Part I of paper. This issue.
- [3] Migliori A, Sarrao JL, Visscher WM, Bell TM, Lei M, Fisk Z, et al. *Physica B* 1993;183:1.
- [4] Chu F, Lei M, Maloy SA, Petrovic JJ, Mitchell TE. *Acta Mater* 1996;44:3035.
- [5] He Y, Schwarz RB, Migliori A, Whang SH. *J Mater Res* 1995; 10:1187.
- [6] Chu F, Lei M, Migliori A, Chen SP, Mitchell TE. *Phil Mag B* 1994;70:867.
- [7] Chu F, He Y, Thoma DJ, Mitchell TE. *Scripta Metall Mater* 1995;33:1295.
- [8] Thoma DJ, Chu F, Peralta P, Kotula PG, Chen KC, Mitchell TE. *Mater Sci Eng* 1997;A239-240:251.
- [9] Chen KC, Allen SM, Livingston JD. *Mater Sci Eng* 1998; A242:163.
- [10] Kronberg ML. *Acta Metall* 1957;5:507.
- [11] ASTM E384-89.
- [12] Anstis GR, Chantikul P, Lawn BR, Marshall DB. *J Am Ceram Soc* 1981;64:533.
- [13] Lawn BR, Marshall DB. *J Am Ceram Soc* 1979;62:347.
- [14] Courtney TH. *Mechanical behavior of materials*. New York: McGraw-Hill, 1990.
- [15] Livingston JD, Hall EL. *J Mater Res* 1990;5:5.
- [16] Thoma DJ, Chu F, Wills JM, Mitchell TE. High-temperature ordered intermetallic alloys VII. *MRS Symp Proc* 1997;460: 689.
- [17] Simmons G, Wang H. *Single crystal elastic constants and calculated aggregate properties: a handbook*. Cambridge, MA: MIT Press, 1971.
- [18] Smithells CJ, Brandes EA, editors, *Smithells metals reference book*. London: Butterworth, 1978.
- [19] Paufler P. *Chemische Gesellschaft* 1984;9:175.
- [20] Paufler P, Eichler K, Schulze GER. *Monatsberichte* 1970;12: 949.
- [21] Westbrook JH. In: Westbrook JH, editor. *Mechanical properties of intermetallic compounds*. John Wiley & Sons, 1960.
- [22] Fleischer RL. *Scripta Metall Mater* 1992;27:799.
- [23] Hazzeldine PM, Pirouz P. *Scripta Metall Mater* 1993;28:1277.
- [24] Chu F, Pope DP. *Mater Sci Eng A* 1993;170:39.
- [25] Takasugi T, Yoshida M, Hanada S. *Acta Mater* 1996;42:669.
- [26] Rice J, Thomson D. *Phil Mag* 1974;29:73.
- [27] Allen CW, Liao KC, Miller AE. *J Less-Common Metals* 1970; 52:109.
- [28] Foley JC, Thoma DJ, Perepezko JH. *Metall Mater Trans* 1994; 25:230.

[29] Chen KC, Thoma DJ, Kotula PG, Chu F, Cady CM, Gray GT, Dunn PS, Korzekwa, DR, Mercer C, and Soboyejo W. In: The Third Pacific Rim International Conference on Advanced Materials and Processing (PRICM 3), 1998. p. 1431.

[30] Liu CT, Zhu JH, Brady MP, McKamey CG, Pike LM. *Intermetallics* 2000;8:1119.

[31] Thoma DJ, Perepezko JH. *J Alloys and Compounds* 1994; 224:330.